TU Delft

Delft University of Technology

Document Version
Final published version

Licence
Dutch Copyright Act (Article 25fa)

Citation (APA)
Ferro, A., Van der Wal, E., Puspitasari-Kokko, A., Lathouwers, D., Hoogeman, M., Sacchi, R., Vignati, A., & Rovituso, M. (2026). A fully 3D-printed contoured double passive scattering system for ultra-high-dose-rate irradiations. *Physica Medica*, *145*, Article 105770. https://doi.org/10.1016/j.ejmp.2026.105770

Important note
To cite this publication, please use the final published version (if applicable).
Please check the document version above.

Copyright
In case the licence states “Dutch Copyright Act (Article 25fa)”, this publication was made available Green Open Access via the TU Delft Institutional Repository pursuant to Dutch Copyright Act (Article 25fa, the Taverne amendment). This provision does not affect copyright ownership.
Unless copyright is transferred by contract or statute, it remains with the copyright holder.

Sharing and reuse
Other than for strictly personal use, it is not permitted to download, forward or distribute the text or part of it, without the consent of the author(s) and/or copyright holder(s), unless the work is under an open content license such as Creative Commons.

Takedown policy
Please contact us and provide details if you believe this document breaches copyrights.
We will remove access to the work immediately and investigate your claim.

This work is downloaded from Delft University of Technology.

Physica Medica 145 (2026) 105770

Contents lists available at ScienceDirect

Physica Medica

journal homepage: www.elsevier.com/locate/ejmp

A fully 3D-printed contoured double passive scattering system for ultra-high-dose-rate irradiations

A. Ferro [a,b,*], E. Van der Wal [c], A. Puspitasari-Kokko [c], D. Lathouwers [d], M. Hoogeman [c], R. Sacchi [a,b], A. Vignati [a,b], M. Rovituso [c]

[a] Università degli Studi di Torino, Dipartimento di Fisica, via P. Giuria 1, Torino, Italy
[b] INFN, sezione di Torino, via P. Giuria 1, Torino, Italy
[c] Department of Research and Development, HollandPTC, Delft, the Netherlands
[d] Technical University of Delft, the Netherlands

ARTICLE INFO

Keywords:
Ultra-high dose rate (UHDR)
FLASH radiotherapy
Proton therapy
Passive scattering
3D-printed contoured scatterer
TOPAS Monte Carlo simulation
Field uniformity

ABSTRACT

Ultra-High Dose-Rate (UHDR) Proton Therapy is an area of active research due to its potential to target cancer cells while sparing healthy tissues. To deepen the knowledge of underlying biological mechanisms of FLASH effect, pre-clinical experiments are required, necessitating large uniform field achieving dose rates above 40 Gy/s. To achieve this, in the Research & Development (R&D) fixed horizontal proton beam line of HollandPTC, a fully 3D printed contoured passive scattering system has been developed. This system is designed to shape a 250 MeV proton beam into a suitable configuration for pre-clinical radiobiological experiments, achieving the necessary dose rates and uniform field distribution. The beamline configuration was initially modelled using the Monte Carlo-based Tool for Particle Therapy Simulation (TOPAS). Subsequently, the contoured passive scattering system was optimized through simulations to generate a sufficiently uniform field for future radiobiological experiments. To validate simulations, the system was fabricated using advanced 3D printing technology. A tungsten-heavy filament blend, consisting of approximately 75% tungsten by mass, was employed in a fused deposition modelling (FDM) process. Simulations were validated against experimental data. The measured dose distributions demonstrated a lateral field uniformity exceeding 95%, corresponding to a dose homogeneity within ± 3% over a field diameter of 2.8 cm. Dose rates above 40 Gy/s were achieved under experimental conditions, with measured values reaching up to approximately 60 Gy/s at the beam entrance, and 100 Gy/s within the Spread-Out Bragg Peak (SOBP). These results confirm the system's design and performance, thus opening multiple possibilities for UHDR radiobiological experiments.

1. Introduction

Proton therapy has long been recognized for its precision in targeting tumors, minimizing damage to surrounding healthy tissues due to its unique depth-dose distribution. In recent years, a new technique called FLASH-radiotherapy has garnered significant attention for its potential to further enhance therapeutic outcomes. FLASH-radiotherapy involves delivering UHDR, typically exceeding 40 Gy/s, resulting in irradiation times on the order of milliseconds. Several preclinical studies have been shown to trigger the "FLASH effect," a phenomenon in which normal tissues experience reduced radiation-induced toxicity while maintaining effective tumor control [1–5]. If confirmed in clinical settings, this phenomenon could represent a significant step forward in minimizing side effects compared to conventional proton therapy.

Despite the promising clinical potential of proton FLASH, the underlying biological mechanisms of the FLASH effect remain poorly understood. It is hypothesized that the differential response between healthy and tumor tissues to UHDR radiation may involve complex biochemical pathways, but further research is necessary to validate these assumptions [6,7]. Pre-clinical studies, involving both radiobiological experiments and the development of advanced technological systems, are essential for optimizing FLASH protocols and transitioning from experimental to clinical use [8].

A key challenge in the advancement of FLASH-radiotherapy is the development of systems capable of delivering these ultra-high dose rates while maintaining accurate dosimetry. This requirement applies across

* Corresponding author.
E-mail address: a.ferro@unito.it (A. Ferro).

https://doi.org/10.1016/j.ejmp.2026.105770
Received 9 September 2025; Received in revised form 9 January 2026; Accepted 14 March 2026
Available online 18 March 2026
1120-1797/© 2026 Published by Elsevier Ltd on behalf of Associazione Italiana di Fisica Medica e Sanitaria.

different delivery configurations, including both gantry-based clinical systems and fixed horizontal beamline R&D setups, which must be equipped with dedicated instrumentation to ensure accurate dose measurement, dose uniformity, and reliable monitoring at high dose rate. Addressing these challenges will enable high-quality pre-clinical experiments and eventually facilitate clinical implementation. Over the past few years, several research centers worldwide have reported on the development of FLASH-capable irradiation platforms, describing a range of technical solutions based on modified clinical beamlines, dedicated experimental setups, or alternative beam delivery strategies [9–12]. These approaches differ in terms of beam delivery technique, achievable field size, dose uniformity, and system complexity, reflecting the diverse constraints and design adopted at different facilities.

In particular, several proton FLASH implementations rely on either scanning-based delivery with limited field sizes or on passive scattering solutions that often require complex or facility-specific hardware modifications. While these approaches have demonstrated the feasibility of proton FLASH irradiation, achieving large, laterally uniform fields at UHDR conditions in a simple, flexible, and reproducible manner remains an open challenge for pre-clinical research.

In this context, a double passive scattering system has been specifically designed and implemented at HollandPTC for their fixed horizontal experimental beamline. The system relies exclusively on passive scattering techniques and supports large-field, variable-size irradiation, making it suitable for a wide range of pre-clinical studies, including *in vitro* and *in vivo* experiments, as well as dosimetric validation studies, such as the verification of dose delivery, field uniformity.

Passive scattering systems offer a simple and efficient approach for UHDR delivery without the temporal constraints associated with scanning-based delivery [13,14]. However, they face limitations in simultaneously achieving the high dose rates and large uniform fields required for pre-clinical radiobiological experiments.

In this work, we aim to further develop and validate a novel contoured double-scatterer system, optimized for FLASH proton therapy research at 250 MeV on the HollandPTC R&D beamline. Our design offers the advantages of being easy to fabricate, straightforward to align, and versatile enough to be adapted to different beamline facilities. The system utilizes fully 3D-printed components and includes a uniform first scatterer along with a bi-material second scatterer. By simulating and experimentally validating this setup using the TOPAS toolkit, we demonstrate its capability to achieve at least 95% field uniformity for a 3 cm diameter field, meeting the requirements for radiobiological applications under UHDR conditions.

2. Materials and methods

2.1. TOPAS simulation of the proton beamline

The TOPAS toolkit (Version 3.9), based on the Monte Carlo platform Geant4, was employed to simulate the experimental setup, including geometry, materials involved, physics process regulating particle interactions, and the visualization of particle trajectories [15,16]. The six default modules of the TOPAS "Physics-List" were used to define the interaction types and the atomic or nuclear physics parameterizations, ensuring an accurate description of the physical processes. Particle transport was simulated using the default TOPAS electromagnetic physics models. Production cuts were set to the default TOPAS values for photons, electrons, positrons, and protons, corresponding to the standard Geant4 range cut configuration. To ensure accurate modelling of multiple Coulomb scattering and energy deposition within the scatterer components and scoring regions, the maximum step size was limited to 0.2 mm in these volumes, while default TOPAS step limits were used elsewhere. Dose scoring was performed in water-equivalent volumes positioned downstream of the double-scatterer system. Each simulation consisted of 1×10^8 primary protons, yielding statistical uncertainties below 1% in the scored dose distributions. No variance reduction techniques were applied. All TOPAS simulations were performed on the HollandPTC computer cluster.

The Monte Carlo modelling approach employed in this study builds upon the validated framework previously reported in Ref. [17], where the HollandPTC fixed horizontal research beamline was characterized over a range of proton energies. In the present work, the same modelling strategy is adopted and further specialized for a proton energy of 250 MeV, corresponding to the energy used for the optimization and experimental validation of the proposed FLASH irradiation system.

Table 1 outlines key geometric elements that define the behaviour of the 250 MeV protons in the simulation. The non-symmetrical Gaussian pencil proton beam of HollandPTC R&D beamline was optimized using a six-parameters model emerging after the Kapton vacuum pipe exit window (thickness: 0.25 mm). This model includes two lateral beam spot sizes (σ_x, σ_y), two angular spreads (ϑ_x, ϑ_y), the initial mean energy (E_0), and the energy spread (Δ E) parameters. The beam source parameters were iteratively adjusted to closely match the simulated beam with experimental data.

All proton experiments are conducted in the experimental room at HollandPTC, with the setup shown in Fig. 1.

The first step involved the optimization of the lateral beam spots size and angular spreads. In this context, the 250 MeV proton pencil beam envelope was measured with the Lynx detector (IBA Dosimetry, Schwarzenbruck, Germany) under free-in-air conditions at different positions (9), covering most of the radiation field downstream from exit window (0 – 250 cm), as shown in Fig. 2-a.

Both experimental and simulated beam profile data were fitted with a Gaussian function to determine the sigma values in X and Y directions. Specifically, the output of the Lynx detector is a 2D image, as shown in Fig. 3. The images were analysed using a 2D Gaussian fit to model and characterize the proton beam. From this fit, 1D cross-sectional profiles were extracted along both X-axis and Y-axis, passing through the centre of mass of the distribution. The software analysis provided information on the misalignment (in mm), sigma values of the distribution and the beam asymmetry percentage, both in 1D central sections and 2D Gaussian fitting.

In the second step, the initial mean energy E_0 and energy spread Δ E, were optimized against the experimental depth-dose profiles of 250 MeV protons. Experimental measurements of the depth-dose profiles were obtained with Qubenext (DE.TEC.TOR, Turin, Italy) positioned at the beam isocentre which is 91.1 cm from the exit window as can be seen in Fig. 2b). A 10 cm thick slab of water equivalent RW3 material was placed in front of the Qubenext, because its dimensions would not fully cover the range of 250 MeV protons.

2.2. Contoured scatterer design

From the Kapton exit window of the beamline the initially narrow Gaussian proton beam, needs to be broadened to cover larger uniform areas [18]. To achieve this, a contoured double scattering system was used. The system includes a first scatterer (FS) made of high-Z material, placed 2 cm from the exit window. The Gaussian lateral distribution of the proton beam is broadened by Multiple Coulomb Scattering (MCS)

Table 1
Characteristics of the geometric elements implemented in the simulation for the beam modelling.

Name	Dimensions	Material
Kapton vacuum pipe exit window	Cylinder (diameter, z): 100, 0.25 mm	G4_KAPTON
Beam monitor BMI07 DE.TEC.TOR	Box (x, y, z): 300, 300, 0.6 mm	G4_WATER
Lynx detector IBA	Box (x, y, z): 300, 300, 0.4 mm	G4_AIR
Qubenext DE.TEC.TOR	Box (x, y, z): 127, 127, 400 mm	G4_WATER

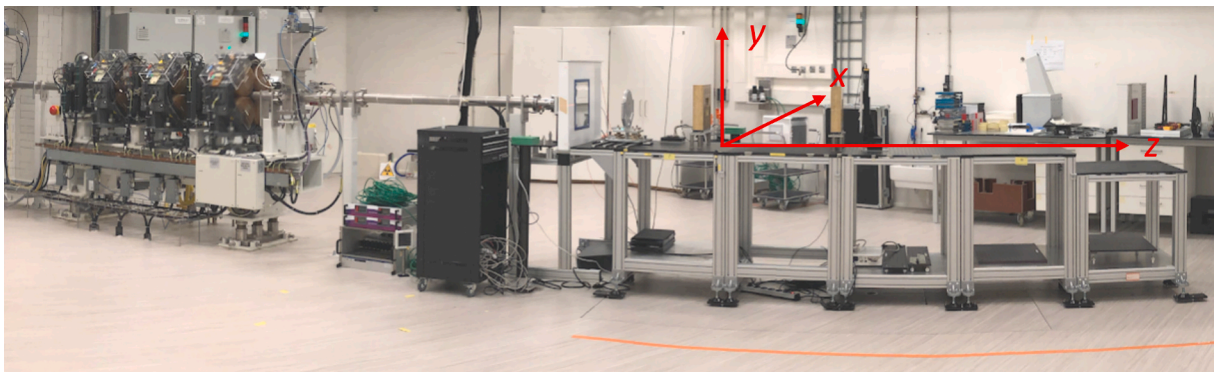


Fig. 1. The experimental room of HollandPTC houses a fixed horizontal proton beamline. The setup includes room lasers for precise alignment. Monitoring systems are mounted on sliding guides positioned immediately downstream of the exit window. Shown in red is the reference system that will be used in the subsequent sections to describe the experimental setup and the analysis of the results. (For interpretation of the references to colour in this figure legend, the reader is referred to the web version of this article.)

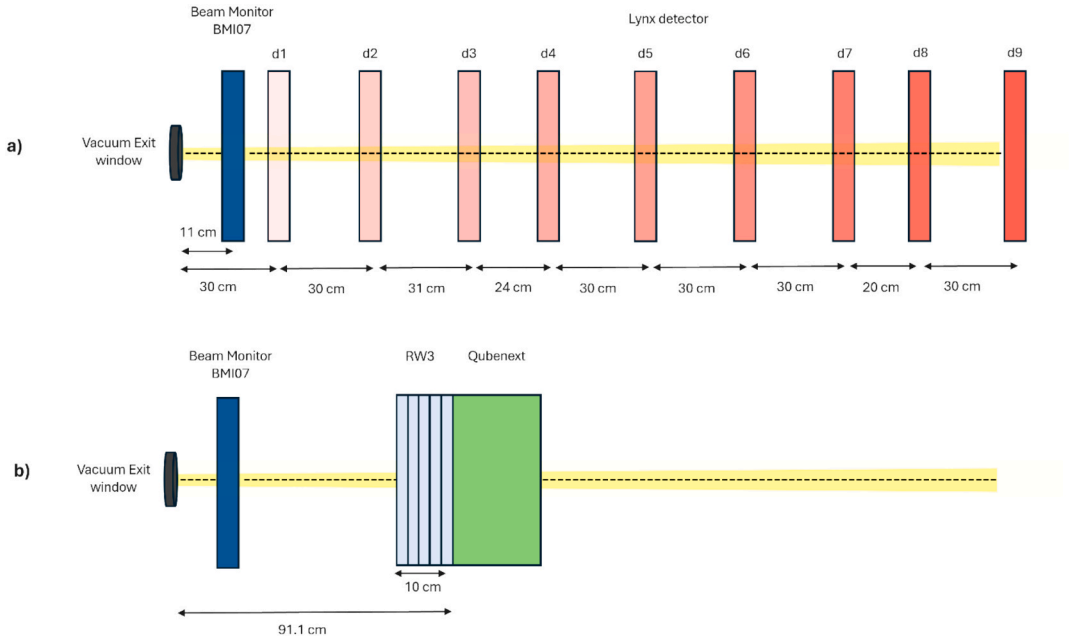


Fig. 2. Scheme of the experimental setup to describe the beam. Source. The BMI07 ionization chamber (DE.TEC.TOR, Turin, Italy) is always positioned downstream the exit window to monitor the beam. a) The positioning of the Lynx detector at nine different distances (d1 – d9) along the beam path is illustrated. b) The Qubenext (DE.TEC.TOR, Turin, Italy) was positioned at the beam isocentre after 10 cm of RW3 to measure the dose-depth distribution of the 250 MeV proton beam.

when interacting with the first scatterer [19]. A second contoured, bi-material scatterer (SS) is positioned 65 cm downstream to further broaden and flatten the lateral beam distribution, making the beam larger and more uniform. Further theoretical details can be found in reference [20].

The design of the contoured scatterer was finalized following an extensive review of the literature, particularly as described in [30]. The optimization was performed using a stepwise, physics-driven approach based on Monte Carlo simulations. Several parameters had to be optimized, including the thickness of the object in the two materials used, as well as the Gaussian profile width of both the upper surface (pink part in Fig. 4) and the cavity on the lower surface (orange part in Fig. 4). In a first step, the longitudinal position of the scattering system along the beamline was defined to ensure compatibility with existing and future experimental components. Subsequently, the Gaussian-shaped cavity at the base of the second scatterer was sized to match the measured lateral dimensions of the 250 MeV proton beam downstream of the first scatterer. The experimentally determined beam width was used as a fixed input parameter to define the cavity profile. In a second step, the remaining geometrical parameters of the contoured scatterer, including the Gaussian width of the upper surface and the thickness distributions of the high-Z and low-Z regions, were initially scaled according to reference values reported in the literature. These parameters were then iteratively adjusted using Monte Carlo simulations to compensate for energy loss and scattering effects, with the objective of achieving a laterally uniform dose distribution. The optimization criterion was defined as achieving a flat dose profile with a diameter of 3 cm, corresponding to a lateral dose uniformity of at least 95%, while minimizing fluence loss in order to preserve ultra-high dose rates at the target.

To balance lateral beam broadening and energy loss, the second scatterer combines high-Z and low-Z materials. Protons traversing the central region of the SS experience a larger material thickness and therefore lose more energy than those passing through the peripheral regions, resulting in a flattened lateral dose distribution [10]. PETG was selected for the low-Z material, and a mixture of 75% tungsten with PETG was used for the high-Z material. This configuration not only flattens the beam profile but also minimizes fluence loss maintaining a high dose rate at the target. By carefully tailoring the thickness and

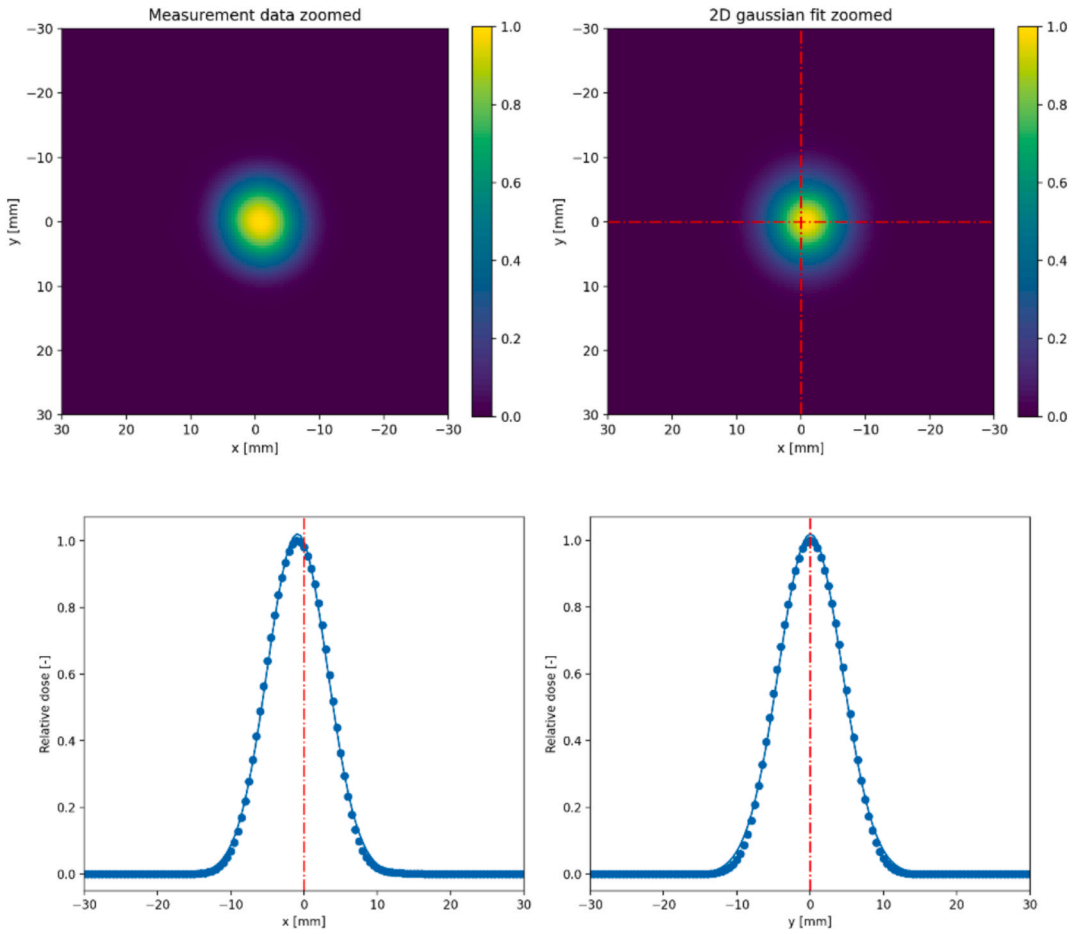


Fig. 3. The output images acquired from the Lynx detector are presented. In the first row, the spatial distribution of the proton beam is shown using a color-coded map, with the dashed red line representing the centre of the coordinate system from which the misalignment will be calculated. The last row displays the 1D cross-sectional profiles of the distributions, derived from the centre of mass and fitted with a Gaussian function. (For interpretation of the references to colour in this figure legend, the reader is referred to the web version of this article.)

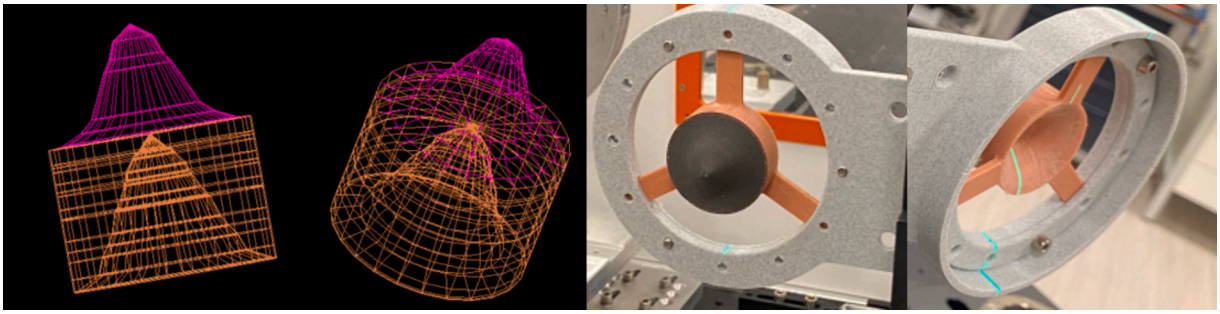


Fig. 4. A comparison between the contoured scatterer layout implemented in TOPAS and its physical realization via 3D printing is shown. On the left, the pink section corresponds to the grey upper part of the 3D-printed scatterer, while the orange section represents the lower part. On the right, a 3D-printed support is also shown, designed to facilitate the alignment of the scatterer during the experiments. (For interpretation of the references to colour in this figure legend, the reader is referred to the web version of this article.)

material composition of the second scatterer, the proposed design minimizes the reduction in the number of protons contributing to the useful irradiation field at the target, caused by nuclear attenuation, large-angle scattering, and geometric losses within the scattering system, thereby preserving a high proton fluence at the target and maintaining the ultra-high dose rates required for FLASH irradiation. Since proton scattering and energy loss depend on the beam energy, this double passive scattering system is effective for mainly one proton energy. The FS and SS components were incorporated into a model, with Table 2. detailing the system's specifications (dimensions, materials) for a 250 MeV proton beam.

After designing the setup in TOPAS, the scatterer was produced in-house using fused deposition modelling (FDM) 3D printing [21,22]. The contoured scatterer geometry was directly exported from the Monte Carlo model and converted into a printable CAD file. The components were printed using PETG filament for the low-Z regions and a tungsten-loaded PETG filament (75% tungsten by weight) for the high-Z regions.

Printing was performed with a layer-by-layer deposition process

Table 2
Geometry of the double passive scattering system implemented in the beamline.

Name	Dimensions	Material
First scatterer (FS)	Cylinder (diameter, z): 50, 5 mm	PETG + 75% tungsten
Contoured scatterer (SS)	Upper part (diameter, z): 40, 22 mmLower part (diameter, z) : 40, 30 mm	PETG + 75% tungsten PETG

using a nozzle diameter of 0.4 mm and a layer height of 0.2 mm, selected to ensure an adequate compromise between geometric accuracy and printing time. A solid infill was used to guarantee material homogeneity and mechanical stability. After printing, the scatterer dimensions were verified using calliper measurements to confirm agreement with the design specifications within ± 0.1 mm.

The modular design and the use of standard FDM printing technology allow the scatterer to be fabricated rapidly and reproducibly in-house, without the need for specialized manufacturing facilities.

Fig. 4 illustrates the comparison between the topas design and the final 3d-printed scatterer.

2.3. Contoured field characterization

In the design of the double scattering system, the goal was to achieve a dose rate above 40 Gy/s on a field of at least 3 cm diameter, with a dose uniformity of at least 95% across the field area. These criteria are consistent with the field sizes and dose rates typically employed in preclinical FLASH radiobiological studies reported in the literature [23]. Importantly, a field size of this scale enables radiobiological investigations beyond highly localized or partial irradiations, supporting whole-tumour irradiation, tissue-sparing studies, immunological endpoints, and in-vitro experiments requiring uniform irradiation of extended sample areas. Such capabilities are essential for enhancing the translational relevance of proton FLASH research.

The field uniformity (U) across the field, for both the experimental and simulated data, was calculated by:

$$U = \left(1 - \frac{I_{max} - I_{min}}{I_{max} + I_{min}}\right) \cdot 100\%$$

where I_{max} and I_{min} are the maximum and the minimum intensity across the plateau region selected respectively.

The validation of the model involves the comparison of simulated and experimental data. The initial alignment of the scatterer is performed using the room laser system, but double scattering systems are strongly affected by alignment with respect to the beam, which becomes a critical parameter to produce a uniform flat field of certain dimension. For this reason, the contoured scatterer was fixed on a holder mounted on a linear motor stage that can move the object with a precision of 0.001 mm in X-Y directions (being Z the beam direction).

The passive scattering system was positioned on the table as described in Fig. 5. As described in part a) a Lynx detector, positioned at 110 cm from the exit window, was employed to measure lateral dose profiles.

After every measurement the data was processed with analysis scripts to get the field dimension and the uniformity and so the alignment evaluated.

Depth dose profiles were measured using the Qubenext detector, as described in Fig. 5b). To create a SOBP, a 2D range energy modulator of low-Z material was inserted. The modulator available in the R&D beam line was used to this purpose.

Since the focus is on relative dose, all dose profiles were normalised to the corresponding maximum dose.

Finally, the dose rate was measured with a parallel-plate Advanced Markus ionization chamber (PTW, Germany). Measurements were carried out at the mid-SOBP depth, which was reached by placing slabs of RW3 water-equivalent material upstream of the chamber. The chamber

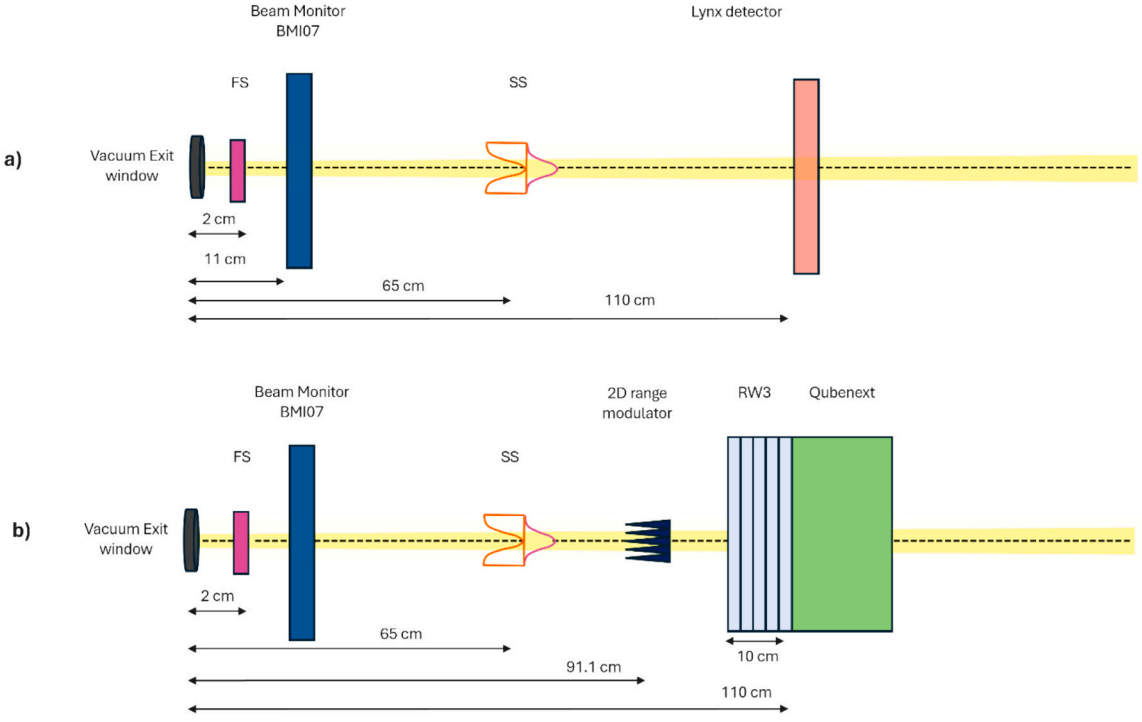


Fig. 5. Schematic representation of the experimental setup with the implemented double passive scattering system. The key components are shown, including the first scatterer (FS), the contoured second scatterer (SS). High-Z materials are shown in pink, while low-Z components are in orange. The measurement devices are illustrated downstream. a) Experimental setup for lateral dose profile measurements. b) Setup for depth dose profile measurements. (For interpretation of the references to colour in this figure legend, the reader is referred to the web version of this article.)

was positioned at the beam isocentre and aligned with the beam central axis.

The absorbed dose to water was derived according to standard ionization chamber dosimetry formalism:

$$D_{w,Q} = M \cdot N_{D,w} \cdot k_Q \cdot k_s \cdot k_{pol},$$

where M is the chamber reading corrected for temperature and pressure. For the Advanced Markus chamber (serial number SN002231), the calibration and correction factors were:

$N_{D,w} = 1.526$ Gy/nC, $k_Q = 1.002$, $k_s = 1.0009$, and $k_{pol} = 1.0024$.

Dose profiles along beam central axis in a water phantom were simulated in TOPAS with a spatial resolution of 1 mm in both lateral and depth bins.

3. Results

3.1. Source model optimization

The beam source parameters in TOPAS, including the lateral beam spot size (σ_x, σ_y) and angular spread (ϑ_x, ϑ_y), were optimized to reproduce the experimental beam envelope data of the 250 MeV proton beam.

The beam's lateral shape was simulated at nine different positions in air and subsequently compared with corresponding experimental data. At each position, a Gaussian fit was applied to the data to extract the sigma values of the distribution, representing the beam's spread, as shown in Fig. 6.

The beam source parameters were iteratively adjusted to closely match the simulated beam's lateral spread and angular distribution with experimental data. Fig. 7, illustrates the final agreement between the simulation and experimental data, with the following lateral beam spots size and angular deviations: $\sigma_x = 2.54$ mm, $\sigma_y = 1.92$ mm, $\vartheta_x = 0.0022$ rad, $\vartheta_y = 0.0028$ rad.

3.2. Pristine Bragg peak verification

The pristine Bragg Peak curve was measured using the Qubenext to benchmark the TOPAS beam source model. Reproducing the Bragg curve is essential in order to get the correct initial energy, and the energy spread.

After an iterative process, optimal values of $E_0 = 249$ MeV and $\Delta E = 0.7$ MeV were found to provide the closest match between the simulations and experimental data.

The bin size in the TOPAS simulation was set to 1 mm to generate high-resolution data, represented by the red points in Fig. 8. In comparison, the experimental data collected with the Qubenext detector (black triangles). Starting from a pitch precision of 2.4 mm in water equivalent, the interpolation improved the resolution to 0.5 mm [24]. The simulations and the experimental data presented in Fig. 8 show a very good agreement.

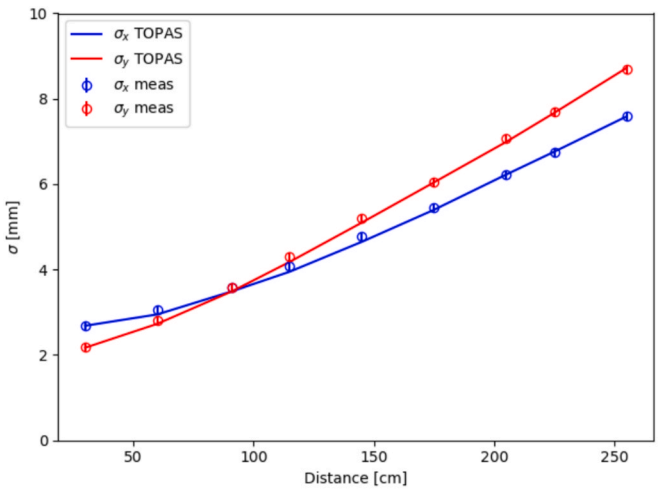


Fig. 7. A comparison between the simulated and experimental beam envelopes of the 250 MeV proton beam is presented. The experimental measurements were obtained using the Lynx detector. The figure shows the spatial spread of the beam as a function of position.

3.3. Experimental validation of the contoured scatterer field

After simulating and validating the beam source parameters, the contoured scatterer design was implemented in the simulations and the best parameters in terms of dimension and distances have been found. Once the contoured scatterer was 3D printed, the experiments have been carried out to find out the field size, uniformity and dose rate achieved.

The validation process involved positioning the dual passive scattering system, as described in section 2.3 with respect to the beam. Experimental data have been acquired using the Lynx detector for the lateral dose profiles.

As previously mentioned in section 2.1 (Fig. 3.), the Lynx detector produces a 2D image where X and Y dose profiles can be extracted or 2D analysis being performed. The target position was chosen to be 110 cm from vacuum exit window, because it gives a good compromise between the desired field size and the wished UHDR.

Fig. 9 illustrates the comparison between the simulated and

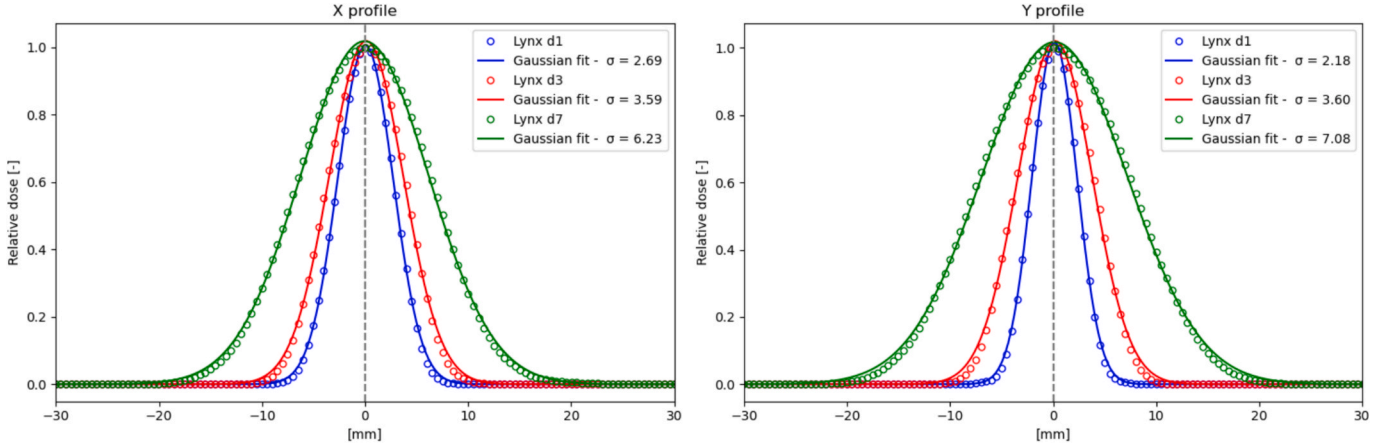


Fig. 6. The beam profiles, measured by the Lynx detector at three different positions d1, d3 and d7 are shown. The measured values are represented by dots, while the dashed line corresponds to the Gaussian fit applied to the data. The extracted sigma is reported in the legend in millimetres.

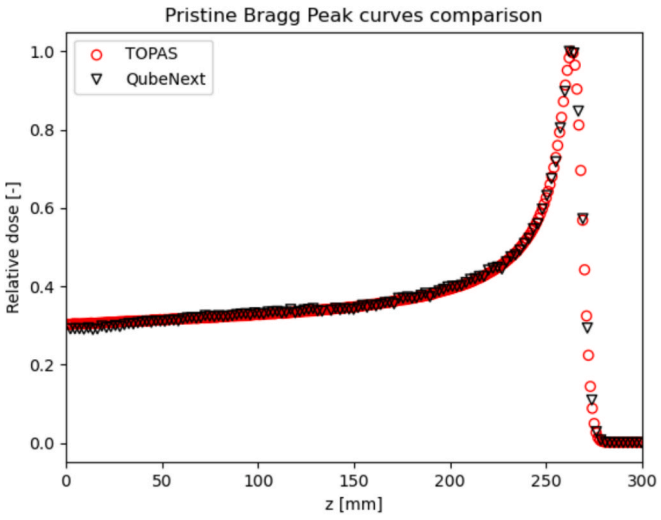


Fig. 8. A comparison between the simulated and experimental dose distributions of the 250 MeV proton beam is shown. The simulated dose distribution, obtained using TOPAS, is represented by red dots, while the experimental dose distribution, measured with the Qubenext detector, is represented by black triangles. (For interpretation of the references to colour in this figure legend, the reader is referred to the web version of this article.)

experimental beam profiles in both directions.

A flat lateral dose profile is crucial for ensuring uniform dose delivery over the target area, particularly in radiobiological application. With 97% of uniformity, a field of 2.8 cm diameter is obtained in both directions.

The comparison between the simulated and experimental results reveals excellent agreement, with a discrepancy of less than 4% between the two data sets. 30.4% of the initial protons end up in the homogeneous region specified.

The measurement was repeated at four additional distances from the beamline exit, which are summarized in the Table 3. For each distance, the experimental field was analysed as described in section 2. These values were then compared with the corresponding simulated results, presented in the adjacent column for reference.

3.4. Depth dose distribution

The dose distributions acquired with the Qubenext detector are displayed in Fig. 10. Fig. 10a) shows the Bragg peak of the 250 MeV passing through the contoured double scattering system without any beam modulation (pristine Bragg peak) and Fig. 10b) shows the resulting SOBP obtained by inserting the 2D range modulator (2DRM) at the isocentre. The 2DRM used in this study is a facility-installed device and it consists of a laterally varying thickness pattern that modulates the proton beam energy across the field, enabling the formation of a SOBP suitable for experimental characterization [23,25].

The pristine Bragg peak represents the characteristic energy deposition profile of the 250 MeV proton beam as it travels through water. In this case, 10 cm of solid water was placed in front of the detector to simulate tissue-equivalent material. The range of the pristine Bragg peak was determined to be 33.6 cm.

In the configuration with the 2D range modulator, with 10 cm of solid water in front of the detector, a 19 mm SOBP plateau is achieved with a 98% dose uniformity. This level of uniformity is crucial for ensuring that the entire target area receives a consistent dose, without significant underdosing or overdosing in any region.

In addition to the lateral beam profiles, the dose rate was measured at each distance at a depth of 10 cm in RW3, using the Advanced Markus ionization chamber.

It is important to note that as the protons travel through air, the lateral spread in both X and Y directions increases. Even if the widening is expected due to scattering effects, however, it comes at the cost of a reduction in dose rate. Finding the desirable balance of the two conditions is critical when planning radiobiological experiments, where both field size and dose rate must meet specific criteria.

Dose rates measurements have been performed over all range of nominal intensities achievable by the cyclotron, from 5nA up 800nA nominal current.

In Fig. 11, the dose rate achievable at a depth of 34 cm in RW3, corresponding to the middle of the SOBP, is shown as a function of the nominal cyclotron current. As expected, and illustrated in the figure, the dose rate increases linearly with the nominal current allowing dose rates up to 100 Gy/s, one of the main pre-requisites of this work.

4. Discussion and conclusions

In this study, we developed and presented a 3D-printed contoured

Table 3
Summary of the field sizes and dose rates measured at entrance of the Bragg Peak, related to position in air.

Distance [cm]	Field size analysed [cm]	Field size simulated [cm]	Dose rate [Gy/s]
110	2.8	2.6	62
120	3.0	2.8	47
140	4.2	4.0	40
155	5.0	4.6	20

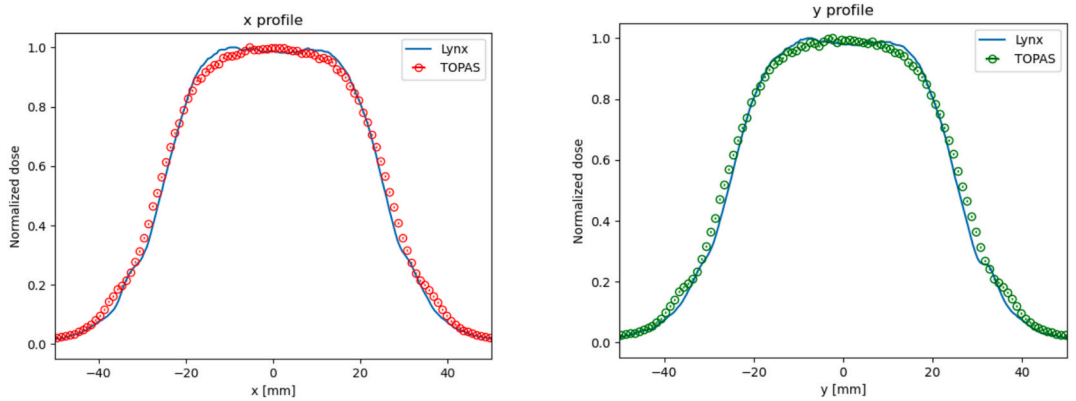


Fig. 9. The validation of the lateral profiles of the 250 MeV proton beam is presented. On the left, the X-axis profile is shown, with the simulated data from TOPAS represented by red dots; on the right, the Y-axis profile is displayed by green dots. The experimental data from the Lynx detector is represented by a blue line. (For interpretation of the references to colour in this figure legend, the reader is referred to the web version of this article.)

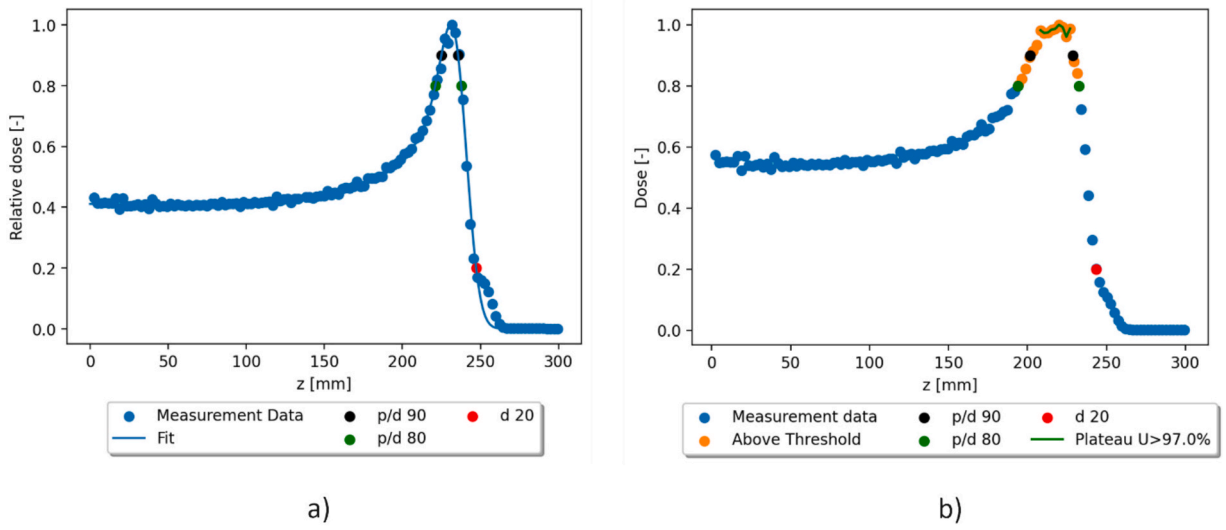


Fig. 10. The differences between two dose distribution curves are presented. a) Shows the Pristine Bragg Peak curve obtained with the contoured passive scattering system; b) displays the SOBP curve with the 2D range modulator inserted, along with the contoured passive scattering system. The analysis software used allows for the identification of the quantities indicated in the legend. The points labelled as "above threshold" present data selected by the analysis software that exceed 70% of the maximum value, highlighting the upper part of the curve, which is the region of interest for determining plateau uniformity.

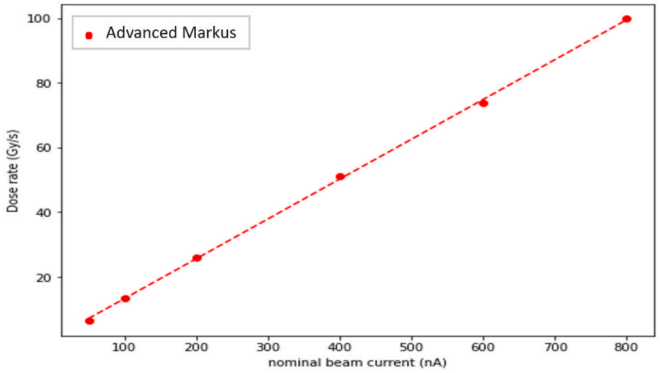


Fig. 11. The dose-rate is plotted as a function of the nominal beam current. The dose rate increases proportionally with the nominal beam current, confirming a linear behaviour of the system. The measured values, obtained with the Advanced Markus detector, are represented by red dots, while the dashed line corresponds to the linear fit of the data.

double scattering system, designed using TOPAS simulations to match the characteristics of the R&D proton beam line at HollandPTC and meet the requirements for UHDR experiments. This system addressed several technical challenges: designing a novel contoured setup that is easy to produce and align with the beam, achieving a minimum field size of 2.8 cm in diameter, and maintaining an average dose rate above 60 Gy/s with a field uniformity exceeding 95%, which is ideal for preclinical studies.

The initial phase of the project focused on constructing the beam source phase space in TOPAS, enabling the integration of the contoured scatterer setup. Simulations of lateral dose profiles and dose rates were conducted to guide the design of a scatterer capable of producing the desired field size and dose rate.

Results from the first stage confirmed the accuracy of the TOPAS model in simulating the behaviour of the experimental proton beam at HollandPTC. The simulation effectively represented both the lateral and depth-wise evolution of the proton beam, thanks to the iterative refinement of parameters such as beam dimensions, angular deviations, initial energy and energy spread. This establishes TOPAS as a robust tool for proton beam simulations, particularly for experimental applications requiring accurate dose distribution and beam evolution predictions. While the present double-scatterer configuration was specifically optimized for 250 MeV, the same design and simulation approach could be adapted to other FLASH-relevant proton energies available at different facilities, requiring a dedicated energy-specific re-optimization of the beam-shaping system. In the validation phase, with the contoured double passive scattering system inserted, a discrepancy of less than 4%, between simulated and experimental lateral dose profiles. This consistency is crucial for ensuring accurate replication of the proton beam's behaviour as it interacts with passive elements and air. The system successfully shaped the proton beam into a uniform, wide dose distribution, with 97% uniformity across a 2.8 cm plateau in both X and Y directions. This performance meets the requirements for radiobiological experiments, where uniform dose distributions are critical.

The contoured double passive scattering system proved to be both effective and simple to fabricate in-house, offering significant flexibility and cost efficiency. This capability eliminates the need for complex and expensive manufacturing processes, allowing for rapid prototyping and customization. Researchers can adapt the system to specific experimental needs or beamline configurations without relying on external suppliers. Moreover, the system's design and fabrication process are highly versatile, making it applicable to a wide range of beamlines. This generalizability enhances its utility across different experimental facilities. Additionally, the ability to fabricate and refine the system in-house facilitates iterative modifications, enabling continuous optimization for improved dose uniformity.

Dose rate measurements further demonstrated the system's capability, with rates reaching up to 100 Gy/s, making it suitable for high-dose-rate applications such as FLASH experiments. As expected, the dose rate exhibited a linear dependence on the accelerator current. This experimental verification confirms that the passive scattering system operates in a stable and predictable manner over the investigated ultra-high dose rate range, supporting its suitability for dynamic experimental conditions.

The effect of inserting a Ridge Filter – a 2D range energy modulator – at the isocentre, producing a 19 mm SOBP plateau with 98% dose uniformity. This high uniformity is essential for clinical and radiobiological applications, where a consistent dose across the target volume is crucial. Further optimization of the Ridge Filter design is planned to enhance the SOBP width, tailoring it to the 250 MeV proton beam for future studies.

The second step visible in Fig. 10, located after the d20, was investigated through TOPAS simulations. It was found to result from the dose released by higher-energy protons compared to those of the main peak (203 MeV, 188 MeV respectively). These protons primarily traversed only the PETG section and were scattered at large angles; in fact, when the scorer size was reduced from 128 × 128 mm^2 to 50 × 50 mm^2, this contribution disappeared, confirming that the secondary peak is due to peripheral scattering.

This study introduces a novel feature to the HollandPTC R&D proton beamline, which is now equipped to conduct UHDR experiments that are ideal for the preclinical studies. This advancement may also benefit other proton beamline facilities operating fixed horizontal research beamlines, by providing a rapidly implementable and flexible solution for pre-clinical FLASH experiments.

Declaration of competing interest

The authors declare that they have no known competing financial interests or personal relationships that could have appeared to influence the work reported in this paper.

References

[1] Wilson P, Jones B, Yokoi T, Hill M, Vojnovic B. Revisiting the ultra-high dose rate effect: implications for charged particle radiotherapy using protons and light ions. Brit J Radiol 2012;85(1018);e933–e939. pMID: 22496068. doi:10.1259/bjr/17827549.

[2] Favaudon V, Caplier L, Monceau V, Pouzoulet F, Sayarath M, Fouillade C, et al. Ultrahigh dose-rate FLASH irradiation increases the differential response between normal and tumor tissue in mice. Sci Transl Med 2014;6:1–10. https://doi.org/10.1126/scitranslmed.3008973.

[3] Montay-Gruel P, Petersson K, Jaccard M, Boivin G, Germond JF, Petit B, et al. Irradiation in a Flash: Unique Sparing of memory in mice after whole Brain Irradiation with Dose rates above 100 Gy/s. Radiother Oncol 2017;124:365–9. https://doi.org/10.1016/j.radonc.2017.05.003.

[4] Vozenin MC, De Fornel P, Petersson K, Favaudon V, Jaccard M, Germond JF, et al. The Advantage of FLASH Radiotherapy Confirmed in Mini-pig and Cat-cancer patients. Clin Cancer Res 2019;25(1):35–42. https://doi.org/10.1158/1078-0432.CCR-17-3375. Epub 2018 Jun 6 PMID: 29875213.

[5] Hageman E, Che P-P, Dahele M, Slotman BJ, Sminia P. Radiobiological Aspects of FLASH Radiotherapy. Biomolecules 2022. https://doi.org/10.3390/biom12101376.

[6] Limoli CL, Vozenin MC. Reinventing Radiobiology in the Light of FLASH Radiotherapy. Annu Rev Cancer Biol. 2023 Apr;7:1-21. doi: 10.1146/annurev-cancerbio-061421-022217. Epub 2023 Jan 11. PMID: 39421564; PMCID: PMC11486513.

[7] Spitz DR, Buettner GR, Petronek MS, St-Aubin JJ, Flynn RT, Waldron TJ, Limoli CL. An integrated physico-chemical approach for explaining the differential impact of FLASH versus conventional dose rate irradiation on cancer and normal tissue responses. Radiother Oncol. 2019 Oct;139:23-27. doi: 10.1016/j.radonc.2019.03.028. Epub 2019 Apr 19. PMID: 31010709; PMCID: PMC6761031.

[8] Hageman E, Che P-P, Dahele M, Slotman BJ, Sminia P. Radiobiological Aspects of FLASH Radiotherapy. Biomolecules 2022. https://doi.org/10.3390/biom12101376.

[9] Jolly S, Owen H, Schippers M, Welsch C. Technical challenges for FLASH proton therapy. Phys Med 2020. https://doi.org/10.1016/j.ejmp.2020.08.005.

[10] Deut U, Camperi A, Cavicchi C, Cirio R, Data EM, Durisi EA, et al. Characterization of a Modified Clinical Linear Accelerator for Ultra-High Dose Rate Beam delivery. Appl Sci 2024;14:7582. https://doi.org/10.3390/app14177582.

[11] Lempart M, Blad B, Adrian G, et al. Modifying a clinical linear accelerator for delivery of ultra-high dose rate irradiation. Radiother Oncol 2019;139:40–5.

[12] Diffenderfer ES, Verginadis II, Kim MM, Shoniyozov K, Velalopoulou A, Goia D, et al. Design, Implementation, and in Vivo Validation of a Novel Proton FLASH Radiation Therapy System. Int J Radiat Oncol Biol Phys 2020;106(2):440–8. https://doi.org/10.1016/j.ijrobp.2019.10.049. PMID: 31928642; PMCID: PMC7325740.

[13] Guoliang Zhang and Junliang Wang and Yuenan Wang and Hao Peng. Proton FLASH: passive scattering or pencil beam scanning? IOP Publishing. jan 2021. Physics in Medicine & Biology. doi:10.1088/1361-6560/abd22d. https://dx.doi.org/10.1088/1361-6560/abd22d.

[14] Durante M, Bräuer-Krisch E, Hill M. Faster and safer? FLASH ultra-high dose rate in radiotherapy. Brit J Radiol 2018;91(1082);20170628. pMID: 29172684. doi: 10.1259/bjr.20170628.

[15] Perl J, Shin J, Schümann J, et al. TOPAS: an innovative proton Monte Carlo platform for research and clinical applications. Med Phys 2012;39(11):6818–37.

[16] Agostinelli S, Allison J, Amako K, et al. GEANT4 - a simulation toolkit. Nucl Instrum Methods Phys Res Sect A: Accel, Spec, Detectors Associated Equipment 2003;506(3):250–303.

[17] Groenendijk CF, Rovituso M, Lathouwers D, Brown JMC. A Geant4 based simulation platform of the HollandPTC R&D proton beamline for radiobiological studies. Phys Med 2023;112:102643. https://doi.org/10.1016/j.ejmp.2023.102643. Epub 2023 Jul 30 PMID: 37523926.

[18] Paganetti H. Proton Therapy Physics. 1st ed. Boca Raton, FL: CRC Press; 2016. doi: 10.1201/9780367803551.

[19] Gottschalk B, Koehler AM, Schneider RJ, Sisterson JM, Wagner MS. Multiple coulomb scattering of 160 MeV protons. Nucl Inst and Meth in Phys Res B 1993;74(4):467–90. https://doi.org/10.1016/0168-583X(93)95944-Z.

[20] Grusell E, Montelius A, Brahme A, Rikner G, Russell K. A general solution to charged particle beam flattening using an optimized dual-scattering-foil technique, with application to proton therapy beams. Phys Med Biol 1994. https://doi.org/10.1088/0031-9155/39/12/005.

[21] Esmaili, Ahmad & TERAKAWA, Atsuki & Ishii, Keizo & YAMAZAKI, Hiromichi & MATSUYAMA, Shigeo & KIKUCHI, Youhei & AKIYAMA, Hisaki & KOYATA, Kan & TAGAWA, Atsushi & ITOH, Yuki & YASUNAGA, Shigeyoshi. (2011). A Study on Beam Flattening Based on Compact Double Scatterer Applicable to Rotational Beam Irradiation System in the Proton Therapy Facility at CYRIC, Tohoku University. Progress in Nuclear Science and Technology. 1. 509-512. 10.15669/pnst.1.509.

[22] Paganetti H, Jiang H, Lee SY, Kooy HM. Accurate Monte Carlo simulations for nozzle design, commissioning and quality assurance for a proton radiation therapy facility. Med Phys 2004;31(7):2107–18. https://doi.org/10.1118/1.1762792. PMID: 15305464.

[23] Rohrer Bley C, Wolf F, Gonçalves Jorge P, Grilj V, Petridis I, Petit B, et al. Dose- and Volume-limiting late Toxicity of FLASH Radiotherapy in Cats with Squamous Cell Carcinoma of the Nasal Planum and in Mini Pigs. Clin Cancer Res 2022 Sep 1;28(17):3814–23. https://doi.org/10.1158/1078-0432.CCR-22-0262. PMID: 35421221; PMCID: PMC9433962.

[24] https://hdl.handle.net/11573/542856.

[25] Rovituso M, Groenendijk CF, van der Wal E, van Burik W, Ibrahimi A, Rituerto Prieto H, et al. Characterisation of the HollandPTC R&D proton beamline for physics and radiobiology studies. Phys Med 2025. https://doi.org/10.1016/j.ejmp.2024.104883.